Shear Band Initiation of Brittle Damage Materials

XIN SUN*
Engineering Mechanics Group
Battelle Memorial Institute
Columbus, OH 43201

STEPHANIE A. WIMMER** AND DALE G. KARR†
Department of Naval Architecture and Marine Engineering
The University of Michigan
Ann Arbor, MI 48109-2145

ABSTRACT: Some effects of material degradation on failure mechanisms of brittle damage materials are investigated. Conditions for the localization of deformation within a shear band are established for rate independent damage materials. In contrast with previous work on shear band initiation that relied on plasticity and flow theory formulation, the present study finds it sufficient for the shear band to emerge in the regime of infinitesimal strain for brittle damage materials. Bifurcations from the homogeneous deformation mode in the form of shear bands are captured for loading conditions of plane strain compression and uniaxial compression using conventional continuum damage mechanics formulations. The inclination angle and critical strain for shear band initiation are calculated using well-established mathematical theory. A finite element simulation of shear band initiation for a rectangular mesh deformed in plane strain compression is also presented.

KEY WORDS: brittle damage, strain localization, shear band initiation.

INTRODUCTION

LOCALIZATION OF STRAIN due to shear band formation has attracted considerable attention in the past two decades. Shear bands often play an important role in limiting ductility, and are known to be one of the failure mechanisms for a ductile material. Once a macroscopic shear band forms, very little additional overall straining takes place while large strains accumulate in the band, leading eventually to ultimate fracture. It is possible to explain such localization as the

*Research Scientist.
**Graduate Student Research Assistant.
†Author to whom correspondence should be addressed. Associate Professor.

1056-7895/96/04 0403-19 $10.00/0

result of growth and coalescence of voids that are formed either by debonding or by cracking of second phase particles. In this paper, the inelasticity is due entirely to microcrack formation at infinitesimal strain. We follow the hypothesis of Rudnicki and Rice (1975), that the localization is understood as an instability in the macroscopic homogeneous constitutive description of inelastic materials.

As indicated by many researchers, the predictions of the bifurcation theory for the initiation of the shear bands are very sensitive to the details of the constitutive equations used in the analysis (Rice, 1976; Anand, 1984, Ortiz, 1987). It is well known that the isotropic J_2 flow theory is often too stiff for describing the formation of a shear band at a realistic strain level (Anand, 1984). Gurson (1977) used a continuum constitutive formulation to model the deformation and failure of porous materials. This continuum model for porous plastic materials incorporates the effects of voids through a single scalar parameter, the void volume fraction. By allowing the void growth and dependence of hydrostatic stress, the constitutive relations exhibit plastic dilatancy and pressure sensitivity. These features permit bifurcation from the fundamental deformation mode at experimentally achievable strain levels (Yamamoto, 1978; Tvergaard, 1981). Other constitutive properties such as non-normality, higher yield surface curvature, and vertex formation are also shown to reduce the critical strain for shear band localization (Rudnicki and Rice, 1975; Needleman, 1979; Tvergaard et al., 1981).

Changes to the Gurson constitutive model to account for final growth and coalescence of voids have been proposed by Tvergaard and Needleman (1984). These modifications are based on analyses of interactions and local failure between individual voids (Brown and Embury, 1973; Goods and Brown, 1979). When combined with the constitutive relations, these local failure criteria provide a means of tracking deformation and failure of a continuum element. This modified constitutive model has been employed with this finite element method to analyze ductile failures such as an axisymmetric cup cone fracture (Tvergaard and Needleman, 1984), and shear failure in a plane strain tensile test (Becker and Needleman, 1986). The effect of void nucleation was incorporated in the kinematic hardening model for a porous ductile solid by Tvergaard (1987); also, the effect of a nonuniform distribution of porosity on flow localization and failure in a porous material was analyzed numerically by Becker (1987).

More recently, finite element simulation of shear band formation in plane strain tension and compression has been performed using a dual yield constitutive model by Ramakrishnan and Atluri (1994). In their simulation, the shear band emerges naturally as a solution to the boundary value problem without invoking any instability criterion and it is believed that the reason lies in the constitutive basis supporting a directionally preferred deformation. All of the above studies are based on finite strain and large deformation theory.

On the other hand, damage mechanics is often introduced to study the effects of innumerable, distributed flaws or cavities on its macroscopic mechanical re-

sponse. Within this framework, the effect of damage on the deformation process is taken into account by introducing the damage variables in the constitutive equations (Kachanov, 1958), thus a most important and sensitive aspect of a realistic damage model consists of the establishment of rational damage evolution laws. Due to the overwhelming complexity of the physical phenomenon reflecting the nucleation, growth, and coalescence of microdefects and their interactions, it is difficult, even for simple geometries, to derive the damage evolution laws from a microscopic level (Krajcinovic, 1982; Krajcinovic et al., 1991). Many researchers in this field have focused their attention on finding damage evolution equations and the constitutive equations that will fit the experimental data based on some physical motivation, and very little attention has been paid to material instabilities and quantitative correlations between the stiffness reduction and failure modes of such damaged materials (Kachanov, 1994).

Horii and Nemat-Nasser (1986) used a micromechanics approach to study the failure modes and mechanisms of brittle materials such as rock and concrete. Splitting and faulting were believed to be caused by the interactions of the tension cracks that grow at the tips of the pre-existing cracks. Such failure mechanisms are critical for loading situations in which tensile stresses are dominant. In the following, we address states in which it is assumed that the growth of individual microcracks is locally stable; the instabilities established here are with regard to the loss of the macroscopically homogeneous deformation.

Recently, the localization theory developed by Hill (1958) and Rudnicki and Rice (1975) has been applied to the failure analysis of the so-called plastic-fracturing materials by various authors. This class of materials includes concrete and rocks as well as ceramics and ceramic matrix composites. Ortiz (1987) proposed a theoretical framework for the analysis of localized failure in concrete using an elastic-plastic damage model. Another excellent study has been presented by Neilson and Schreyer (1993) on the general bifurcation theory for elastic-plastic materials. The loss of strong ellipticity criterion was proposed to be used in the place of the classical discontinuous bifurcation criterion as a necessary condition for localization. Examples of localizations have been carried out for infinitesimal deformations of rate and temperature independent materials. Several general experimental observations of necking and localization in metal specimens subject to different boundary conditions are explained using the proposed bifurcation theory and different modes of bifurcation such as diffuse or localized are identified. Also in a recent publication, Neilsen and Schreyer (1992) discussed the bifurcation criteria for elastic damaging materials and used an isotropic scalar damage formulation. Among others are the works of Hild et al. (1992), Pietruszczak and Xu (1995), and Rizzi et al. (1995).

It is the main objective of this study to examine the inception of a shear band along the constitutive path for anisotropic continuum damage models in the regime of infinitesimal strain. We follow the classical discontinuous bifurcation

approach. The mechanical behavior of concrete and ice is modelled using rate independent elastic damage constitutive equations and the tangent moduli of the materials are therefore instantaneous elastic. When a uniform specimen is compressed, the deformation is initially homogeneous. At a particular critical strain, deformation switches from homogeneous to heterogeneous, and thereafter, strains are localized in the shear band region. In this sense, shear band initiation in brittle materials can also be taken as a precursor to brittle fracture. In fact, Krajcinovic and Fonseka (1981) have shown that the thermodynamic force, R, for their parallel bar model actually corresponds to the crack resistance force or the energy release rate.

Finally, a plane strain finite element simulation is presented to illustrate shear band formation during compressive loading. An 8-node 16-d.o.f. element with reduced integration is used and good agreement with the analytical prediction is found. The formation of the shear band can be captured easily as a natural outcome of the simulation, similar to Ramakrishnan and Atluri (1994), without resorting to any instability criterion or "enriched" elements that are employed in come contemporary procedures.

MATHEMATICAL FORMULATION

The bifurcation condition for localization instability is presented for a general three-dimensional brittle solid in this section. We follow the lines of the well-posed mathematical formulation by Rudnicki and Rice (1975) for shear band initiation, only that infinitesimal strain and irrotational deformation are used since strains remain less than 3% on the constitutive path for the continuum damage models used here. The current uniform deformation state is as shown in Figure 1.

We now seek the condition under which nonuniform deformation fields in the form of a planar band may occur. Cartesian coordinates x_i in the shear band local directions are introduced such that the x_1-direction is normal to the planes bounding the band as illustrated in Figure 1. Equilibrium at the onset of localization requires that across the band:

$$\Delta \dot{\sigma}_{1j} = 0, \quad j = 1,2,3 \tag{1}$$

The symbol Δ is used in this paper to denote the difference between the variables inside and outside the band. By the definition of shear band, the velocity field is constrained to vary across the band only:

$$\Delta\left(\frac{\partial v_i}{\partial x_j}\right) = g_i(x_1)\delta_{j1} \quad i,j = 1,2,3 \tag{2}$$

The corresponding strain rates are then given by:

$$\Delta\dot{\epsilon}_{ij} = \frac{1}{2}\left(\Delta\left(\frac{\partial v_i}{\partial x_j}\right) + \Delta\left(\frac{\partial v_j}{\partial x_i}\right)\right) \tag{3}$$

Since we focus our analysis in the regime of infinitesimal strain, it is unnecessary to distinguish between the Kirchhoff stress tensor and Cauchy stress tensor; also, we consider the deformation to be irrotational. The constitutive equation for an elastic material with damage can be written as:

$$\sigma_{ij} = k_{ijkl}(\underset{\sim}{\epsilon}, \underset{\sim}{D})\epsilon_{kl} \tag{4}$$

Taking time derivatives as well as the difference between inside and outside the band, Equation (4) yields:

$$\Delta\dot{\sigma}_{ij} = k_{ijkl}(\underset{\sim}{\epsilon}, \underset{\sim}{D})\Delta\dot{\epsilon}_{kl} + \Delta\dot{k}_{ijkl}(\underset{\sim}{\epsilon}, \underset{\sim}{D})\epsilon_{kl} \tag{5}$$

Substituting Equations (2), (3) and (5) into Equation (1), a set of three homogeneous equations in terms of g_1, g_2, and g_3 are generated.

$$\Delta\dot{\sigma}_{1j} = k_{1j1n}g_n + \frac{\partial k_{1jkl}}{\partial \epsilon_{1n}}\epsilon_{kl}g_n = 0 \tag{6}$$

By definition, the shear band localization can only occur at the first point on the deformation path for which non-zero g_i exist for this set of equations, thus the condition for bifurcation can be found by setting the determinant of the coefficient matrix of g_i in Equation (6) to be zero.

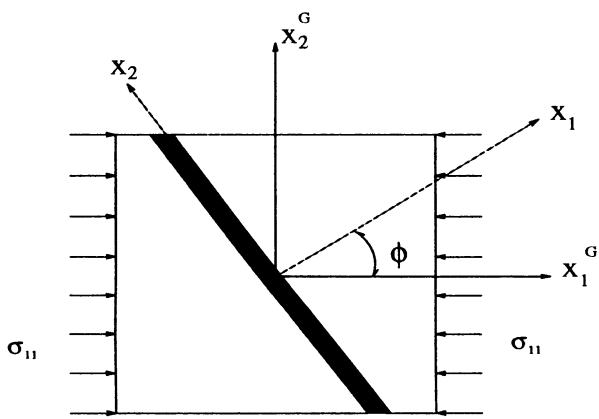

Figure 1. *Illustration of geometry and coordinate convention for plane strain shear band formation.*

An equivalent shear band initiation condition can also be derived from the global coordinate system in accord with the loading condition and the geometry of the specimen. This approach is taken by Tugcu (1993). Introducing the unit normal vector to the shear band surface n_1 the change in stress rate across the band in global coordinate formulations is:

$$\Delta \dot{\sigma}_{ij}^{G} = k_{ijpq}^{G} n_q g_p + \frac{\partial k_{ijkl}^{G}}{\partial \epsilon_{pq}^{G}} \epsilon_{kl}^{G} n_q g_p \tag{7}$$

Therefore, the force continuation condition across the band is:

$$\Delta \dot{\sigma}_{ij}^{G} n_j = 0 \tag{8}$$

Equation (8) is the global equilibrium counterpart of Equation (1). Superscript G is used to distinguish the variables in global coordinates from the variables in local coordinates. In this paper, we will use the above formulations to analyze the possibility of shear band initiation for damage mechanics models under different loading conditions.

The general continuum damage mechanics models are usually derived following the approach of thermodynamical formulations (Davidson and Stevens, 1973; Coleman and Gurtin, 1967). When Helmholtz free energy is chosen with strain as the independent state variable, the general damage evolution equation is of the form:

$$\underset{\sim}{D} = \mathscr{G}(\underset{\sim}{\epsilon}) \tag{9}$$

and the difference in damage rate between the inside and outside of the band at initiation is

$$\Delta \dot{\underset{\sim}{D}} = \mathscr{F}(\Delta \dot{\underset{\sim}{\epsilon}}) \tag{10}$$

The values for strain and damage variables in Equation (5) or (6) can be obtained from the global constitutive path through tensor coordinate transformation:

$$\underset{\sim}{\epsilon} = \underset{\sim}{S} \underset{\sim}{\epsilon}^{G} \underset{\sim}{S}^{T}, \quad \underset{\sim}{D} = \underset{\sim}{S} \underset{\sim}{D}^{G} \underset{\sim}{S}^{T} \tag{11}$$

When Gibbs energy formulation is used with stress as the independent state variable, (see for example, Chow and Yang, 1991, and Kachanov, 1993) increments in strain are related to increments in stress through the tangential compliance tensor:

$$d\epsilon_{ij}^{G} = A_{ijkl}^{G} d\sigma_{kl}^{G} \tag{12}$$

The components of the tangential stiffness tensor used in Equations (6) and (7) are simply related to the inverse of the compliance tensor:

$$d\sigma_{ij}^{G} = L_{ijkl}^{G} d\epsilon_{kl}^{G} \tag{13}$$

The conditions for the shear band formation can therefore be established using expressions (6) or (7) and (8) for either the Helmholtz or Gibbs energy formulations.

We also note that the effects of material element rotation can be included in the analysis by using in Equation (5) the Jaumann differential of σ_{ij} (see Darve, 1984). The condition for strain localization is then:

$$\det \left[n_i L_{ijkl}^{G} n_l + \frac{1}{2} \left(n_p \sigma_{pj}^{G} n_k + n_p \sigma_{pq}^{G} n_q \delta_{jk} - n_p \sigma_{pr}^{G} n_j - \sigma_{jk}^{G} \right) \right] = 0 \tag{14}$$

For the conditions analyzed in the following, however, the error introduced by neglecting the rotational terms in the time derivative of the stress is insignificant.

In the following sections, we provide examples of shear band formation for two particular damage models. The first model is a very simple model in which damage is limited to two principal components and assumed to evolve in proportion to the corresponding principal tensile strain. This model is an extreme simplification of the rate dependent model proposed for polycrystalline ice proposed by Karr and Choi (1989). Failure points corresponding to general bifurcation conditions for the rate dependent ice model have been investigated by Karr and Sun (1995) and Sun (1995). The second model was proposed for concrete by Krajcinovic and Selvaraj (1983). Both models used approximate formulations limited to dilute concentrations of damage (Lubarda and Krajcinovic, 1993). They are studied here to illustrate examples of shear band formation and we should emphasize that such localized deformation modes may be possible regardless of the particular evolution equations employed. Related work and further details of this study are provided in the thesis of Sun (1995) in which the stability of postbifurcation paths are addressed. The distinction between lack of stability and lack of uniqueness of constitutive paths are also addressed for nonlinear models of soils by Darve, Flavigny, and Meghachou (1995).

SHEAR BAND INITIATION FOR TWO-DIMENSIONAL PLANE STRAIN COMPRESSION

As an illustrative example, we use a simple linear damage law, in which damage is assumed to be restricted to two principal planes for uniaxial compression in the x_1 direction:

$$D_{11}^{G} = 0, \quad D_{22}^{G} = \gamma \epsilon_{22}, \quad D_{33}^{G} = \gamma \epsilon_{33} \tag{15}$$

where $\gamma = 200$. The constitutive equation can be written as (Krajcinovic and Fonseka, 1981)

$$\sigma_{ij} = K_{ijkl}\epsilon_{kl} \tag{16}$$

where

$$K_{ijkl} = \lambda\delta_{ij}\delta_{kl} + \mu(\delta_{ik}\delta_{jl} + \delta_{il}\delta_{kj}) + c_1(\delta_{ij}D_{kl} + \delta_{kl}D_{ij}) + c_2(\delta_{jk}D_{il} + \delta_{il}D_{jk})$$

λ and μ are Lamé constants of the virgin material, and c_1 and c_2 are the damage constants to be determined from experiments. Here, we use $\lambda = 8210$, $\mu = 3518.5$, $c_1 = 1370$, $c_2 = -2050$. These are the material constants for polycrystalline ice used by Karr and Choi (1989), Karr and Sun (1995), and Sun (1995).

For plane strain compression loading (as shown in Figure 1), in the global coordinate system, $\epsilon_{33}^G = 0$ and $D_{33}^G = 0$, so the damage and strain tensor simplify, respectively, to

$$\underset{\sim}{D}^G = \begin{bmatrix} 0 & 0 \\ 0 & D_{22}^G \end{bmatrix}, \quad \underset{\sim}{\epsilon}_G = \begin{bmatrix} \epsilon_{11}^G & 0 \\ 0 & \epsilon_{22}^G \end{bmatrix} \tag{17}$$

In the shear band local coordinate system, the in-plane constitutive equations should read:

$$\begin{aligned} \sigma_{11} &= [(\lambda + 2\mu) + 2c_3D_{11}]\epsilon_{11} + [\lambda + c_1(D_{11} + D_{22})]\epsilon_{22} + 2c_3D_{12}\epsilon_{12} \\ \sigma_{12} &= c_3D_{12}\epsilon_{11} + c_3D_{12}\epsilon_{22} + \left[\mu + \frac{c_2}{2}(D_{11} + D_{22})\right]2\epsilon_{12} \end{aligned} \tag{18}$$

where $c_3 = c_1 + c_2$. Taking time derivatives and the difference between inside and outside the shear band, Equation (5) becomes

$$\begin{aligned} \Delta\dot{\sigma}_{11} &= [(\lambda + 2\mu) + 2c_3D_{11}[\Delta\dot{\epsilon}_{11} + [\lambda + c_1(D_{11} + D_{22})]\Delta\dot{\epsilon}_{22} + 2c_3D_{12}\Delta\dot{\epsilon}_{12} \\ &\quad + 2c_3\epsilon_{11}\Delta\dot{D}_{11} + c_1\epsilon_{22}\Delta\dot{D}_{11} + c_1\epsilon_{22}\Delta\dot{D}_{22} + 2c_3\epsilon_{12}\Delta\dot{D}_{12} \\ \Delta\dot{\sigma}_{12} &= c_3D_{12}\Delta\dot{\epsilon}_{11} + c_3D_{12}\Delta\dot{\epsilon}_{22} + \left[\mu + \frac{c_2}{2}(D_{11} + D_{22})\right]2\Delta\dot{\epsilon}_{12} \\ &\quad + c_3\epsilon_{11}\Delta\dot{D}_{12} + c_3\epsilon_{22}\Delta\dot{D}_{12} + \frac{c_2}{2}(\Delta\dot{D}_{11} + \Delta\dot{D}_{22})2\epsilon_{12} \end{aligned} \tag{19}$$

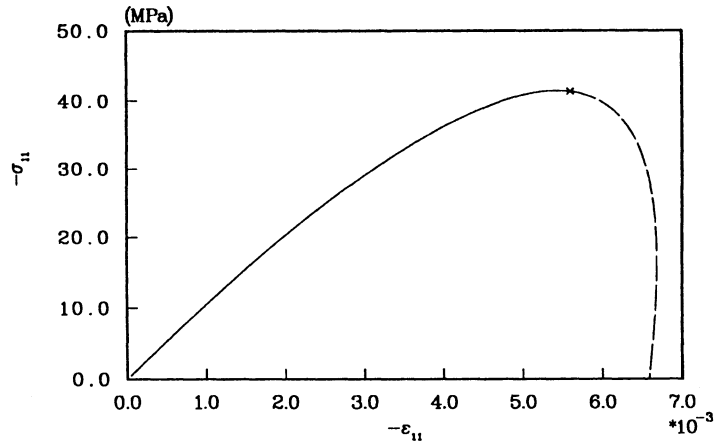

Figure 2. *Compressive stress versus strain for plane strain loading.*

Equation (6) provides the relation

$$\begin{aligned}\Delta\dot{\sigma}_{11} &= [\lambda + 2\mu + 2c_3D_{11} + \gamma(2c_3\epsilon_{11} + c_1\epsilon_{22})]g_1 \\ &\quad + (c_3D_{12} + c_3\gamma\epsilon_{12})g_2 = 0 \\ \Delta\dot{\sigma}_{12} &= (c_3D_{12}) + C_2\gamma\epsilon_{12})g_1 \\ &\quad + \left[\mu + \frac{c_2}{2}(D_{11} + D_{22}) + \frac{\gamma}{2}(c_3\epsilon_{11} + c_3\epsilon_{22})\right]g_2 = 0\end{aligned} \tag{20}$$

Figure 2 shows the compressive stress versus compressive strain for a plane strain specimen in the global coordinate system.

Prior to localization, the nonlinear constitutive equations are easier to solve in the global coordinate system. In order to find the shear band initiation point along the global constitutive path, an in-plane transformation matrix is used. In Equation (11), $\underset{\sim}{S}$ is the in-plane transformation matrix (see Figure 1):

$$\underset{\sim}{S} = \begin{bmatrix} \cos\phi & \sin\phi \\ -\sin\phi & \cos\phi \end{bmatrix} \tag{21}$$

Along the constitutive path, we seek the point at which the determinant of the coefficient matrix in Equation (20) vanishes. The critical strain ϵ_{1crit} and inclination angle ϕ_{crit} for shear band initiation can then be determined by calculating the determinant of the coefficient matrix of Equation (20) for each point along the

constitutive path (Figure 2) for various values of the inclination angle ϕ. Starting from the origin, the first point on the constitutive path that provides a solution for ϕ with the determinant equal to zero is the shear band initiation point and the corresponding ϕ is the inclination angle. For this constitutive model, the critical axial strain and the inclination angle are found to be $\epsilon_{1crit} = -0.00545$ and $\phi_{crit} = 50°$, respectively. In Figure 2, the point corresponding to the shear band initiation is illustrated by a star on the constitutive path.

Hawkes and Mellor (1972) conducted some expression tests on ice slabs to illustrate the internal cracking and final collapse for a compression specimen with laterally restrained ends. The theoretical predicted failure mode presented above agrees with this experimental observation. Brittle failure modes of ice are also discussed and analyzed by Schulson (1990) and Schulson et al. (1989). Both shear faulting and axial splitting occurred and the failure modes are sensitive to the stress states which are in turn dependent upon the end conditions of the specimens. The following section shows that the same damage model used above is subject to axial rupture under uniaxial compression.

SHEAR BAND INITIATION FOR THREE-DIMENSIONAL UNIAXIAL COMPRESSION

Polycrystalline Ice

We follow a similar procedure to analyze the three-dimensional shear band in-

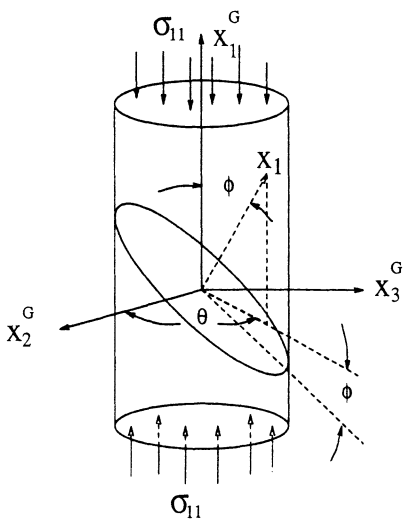

Figure 3. *Illustration of uniaxial loading condition.*

itiation problem. For the loading condition of uniaxial compression as shown in Figure 3, the damage tensor in the global coordinate can be derived from Equation (15). Since $\epsilon_{22}^G = \epsilon_{33}^G$ on the primary constitutive path, the corresponding damage components should also be the same in x_2 and x_3 directions: $D_{22}^G = D_{33}^G = \gamma\epsilon_{22}^G = \gamma\epsilon_{33}^G = D^G$. The damage tensor in the global coordinate system is then:

$$\underset{\sim}{D}^G = \begin{bmatrix} 0 & 0 & 0 \\ 0 & D^G & 0 \\ 0 & 0 & D^G \end{bmatrix} \tag{22}$$

In the shear band local coordinate system (see Figure 3), the combination of Equations (2) and (3) offers the $\Delta\dot{\epsilon}_{ij}$ matrix to be as follows:

$$\Delta\dot{\epsilon}_{ij} = \begin{bmatrix} g_1 & \frac{g_2}{2} & \frac{g_3}{2} \\ \frac{g_2}{2} & 0 & 0 \\ \frac{g_3}{2} & 0 & 0 \end{bmatrix} \tag{23}$$

where g_i are functions of x_1 only. The change in the damage evolution rate, $\Delta\dot{D}_{ij}$ can then be calculated using Equation (15). The constitutive equations in the shear band local coordinate system can be written as follows by expanding Equation (16):

$$\begin{aligned}
\sigma_{11} &= (\lambda + 2\mu + 2c_3D_{11})\epsilon_{11} + [\lambda + c_1(D_{11} + D_{22})]\epsilon_{22} \\
&\quad + [\lambda + c_1D_{11} + D_{33})]\epsilon_{33} + 2c_1D_{23}\epsilon_{23} + 2c_3D_{13}\epsilon_{13} + 2c_3D_{12}\epsilon_{12} \\
\sigma_{12} &= c_3D_{12}\epsilon_{11} + c_3D_{12}\epsilon_{22} + c_1D_{12}\epsilon_{33} + \left[\mu + \frac{c_2}{2}(D_{11} + D_{22})\right](2\epsilon_{12}) \\
&\quad + 2c_2D_{13}\epsilon_{23} + 2c_2D_{23}\epsilon_{13} \\
\sigma_{13} &= c_3D_{13}\epsilon_{11} + c_1D_{13}\epsilon_{22} + c_3D_{13}\epsilon_{33} + \left[\mu + \frac{c_2}{2}D_{11} + D_{33})\right](2\epsilon_{13}) \\
&\quad + 2c_2D_{12}\epsilon_{23} + 2c_2D_{23}\epsilon_{12}
\end{aligned} \tag{24}$$

Taking time derivatives and the difference between inside the outside the band as per Equation (6):

$$\begin{aligned}
\Delta\dot{\sigma}_{11} &= [\lambda + 2\mu + 2c_3D_{11} + \gamma(2c_3\epsilon_{11} + c_1\epsilon_{22} + c_1\epsilon_{33})]g_1 \\
&\quad + [c_3D_{12} + c_3\gamma\epsilon_{12}]g_2 \\
\Delta\dot{\sigma}_{12} &= [c_3D_{12} + c_2\gamma\epsilon_{12}]g_1 \\
&\quad + \left[\mu + \frac{c_2}{2}(D_{11} + D_{22}) + \frac{\gamma}{2}(c_3\epsilon_{11} + c_3\epsilon_{22} + c_1\epsilon_{33})\right]g_2 \\
\Delta\dot{\sigma}_{13} &+ \left[\mu + \frac{c_2}{2}(D_{11} + D_{33}) + \frac{\gamma}{2}(c_3\epsilon_{11} + c_1\epsilon_{22} + c_3\epsilon_{33})\right]g_3
\end{aligned} \tag{25}$$

The strain and damage components in Equation (25) are in the shear band local coordinates. They are found through Equation (11) using a general three-dimensional transformation matrix (see Figure 3):

$$\underset{\sim}{S} = \begin{bmatrix} \cos\phi & \cos\theta\sin\phi & \sin\theta\sin\phi \\ -\sin\phi & \cos\theta\cos\phi & \sin\theta\cos\phi \\ 0 & -\sin\theta & \cos\theta \end{bmatrix} \tag{26}$$

Again, the shear band bifurcation point can be found by setting the coefficient

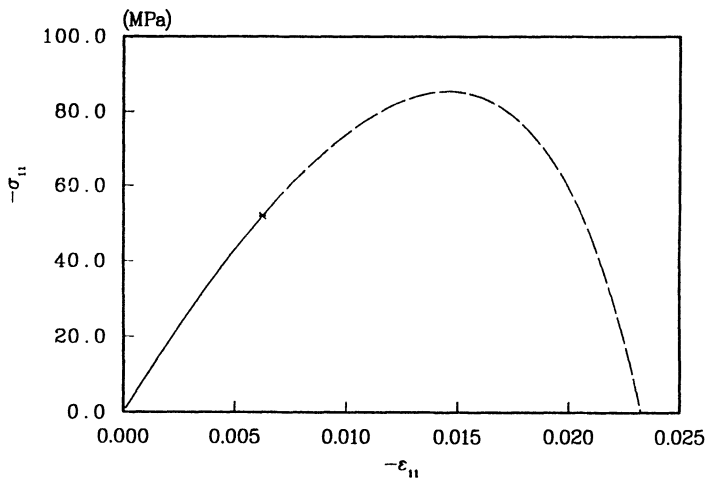

Figure 4. *Stress versus strain for uniaxial compression.*

matrix in Equation (25) to be zero along the constitutive path (Figure 4). For this loading condition, shear band initiation is found to be θ independent due to axial symmetry; the critical strain and the inclination angle of $\epsilon_{1crit} = -0.00625$ and $\phi_{crit} = 90°$, respectively. The bifurcation point is illustrated by a star in Figure 4.

Plain Concrete

As another example, we consider the uniaxial compression test of plain concrete. A set of constitutive equations for concrete were derived by Krajcinovic and Selvaraj (1983) on the basis of the thermodynamical formulation. They assumed a particular form of the Helmholtz free energy, and the stress components are derived as the thermodynamical conjugates to strains as follows:

$$\sigma_{ij} = \varrho \frac{\partial \psi}{\partial \epsilon_{ij}} = k_{ijkl}\epsilon_{kl} \tag{27}$$

where

$$k_{ijkl} = \lambda\delta_{ij}\Delta_{kl} + 2\mu\delta_{ik}\delta_{jl} + C_1(D_pD_p)^{-1/2}(\delta_{ij}D_k^\alpha D_l^\beta + \delta_{kl}D_i^\alpha D_j^\beta)$$

$$+ C_2(D_pD_p)^{-1/2}(\delta_{jk}D_i^\alpha D_l^\beta + \delta_{il}D_j^\alpha D_j^\beta) + 2C_3(D_pD_p)^{-3/2}D_i^\alpha D_j^\beta D_k^\alpha D_l^\beta$$

The thermodynamic forces are derived similarly as conjugates to damage:

$$R_i = -\varrho\frac{\partial \psi}{\partial D_i} = \frac{Ek}{4\sqrt{2}}\left(3K_1 e + 3K_2\epsilon_i + \frac{5}{2}K_3\epsilon_i\right)\epsilon_i, \quad i = 2,3 \tag{28}$$

A dissipation potential similar to the concept of yield surface for plasticity is then assumed. The damage evolution equation is derived based on a normality rule. For the case of uniaxial compression:

$$\dot{D} = CG_0\dot{R}_2 = CG_0\dot{R}_3 \tag{29}$$

The damage then consists of two independent damage systems perpendicular to the lateral strains;

$$D_i^\alpha = D_j^\beta = D, \quad D_1 = 0 \tag{30}$$

In the shear band global coordinate system, the substitution of Equations (27) through (30) into Equations (7) and (8) yields a coefficient matrix similar to Equation (25). Similarly, the shear band bifurcation point was found by setting

the determinant of the coefficient matrix to be zero along the constitutive path. For this loading condition, the critical strain and inclination angle are $\epsilon_{1crit} = -0.00285$ and $\phi_{crit} = 90°$. The bifurcation point is illustrated by a star in Figure 5.

Failure Modes

The eigenvalue problem associated with the classical localization criterion Equation (8) can be quite readily simplified for uniaxial stress conditions (Darve, 1984). The resulting characteristic equation is of second degree in terms of the square in the tan ϕ term. The bifurcation point corresponds to the parabolic boundary between elliptic and hyperbolic regimes. The results here indicating the vertical orientation of the localized band are actually quite similar to the results using plasticity theory obtained for localized necking of sheets under biaxial stretching (Stören and Rice, 1975). The predicted neck formed perpendicular to the axis of maximum principal strain when the two largest principal strains were positive. In the necking studies, the sheets were analyzed for the conditions of plane stress so that the minimum principal strain is compressive. The two analyses are, therefore, also similar to the sense that both situations show a localization band occurring in a plane parallel to the minimum (compressive) axis.

The predicted shear band initiation at $\phi_{crit} = 90°$ corresponds to an axial rupturing mode of failure, this is consistent with many experimental observations for brittle solids in the literature. Hawkes and Mellor (1972) conducted a sequence of uniaxial compression tests on polycrystalline ice. They noted that the failure

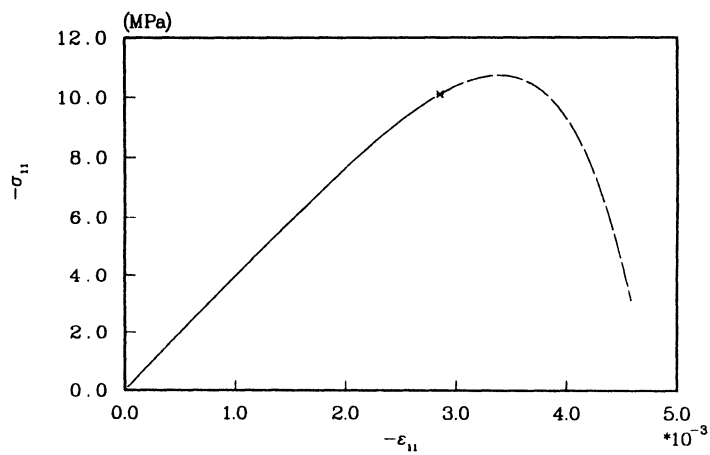

Figure 5. *Stress versus strain for uniaxial compression using elastic constants for concrete.*

mode of uniaxial compression of a cylindrical specimen was always axial cleavage despite the precautions taken, whereas the dumbbell specimens failed by "cataclasis" and "coning." A concrete or rock specimen in unconfined uniaxial compression behaves in a brittle manner and ultimately fails in the splitting mode (Krajcinovic, 1989; Shah, 1984). Experiments on concrete cubes by Mills and Zimmerman (1970) provide more detailed information concerning failure modes of concrete in triaxial stress states. The failed cubes from the uniaxial compression tests were found to be cracked in planes parallel to the loading direction, and the resulting ultimate failure mode was also axial splitting.

Schulson (1990) described the brittle compressive fracture of fresh-water, granular ice. Some of the results of an extensive testing program were explained in terms of the wing crack model developed by Ashby and Hallam (1986). Compressive failure occurred after the samples became heavily damaged by an assembly of cracks of size on the order of the grain size. Full length splitting of the samples occurred through a poorly understood linkage mechanism. One possible trigger for such a mechanism is the loss of (macroscopic) stability of the damaged medium as described in previous subsections. The eigenvectors for both the simplified ice model and the concrete model are tangent to the plane of localization (shear band initiation) and perpendicular to the axial direction. However, after the initiation point for strain localization is reached, the damage evolution for the material inside the shear band is different from the damage evolution for the material outside the band. The post localization behavior of the material within the shear band (see for example, Pietruszczak and Xu, 1995) involving finite deformations leading to full macroscale rupture, is beyond the scope of the damage models presented here, but offers an important extension of the present study.

FINITE ELEMENT SIMULATION OF THE TWO-DIMENSIONAL PLANE STRAIN SHEAR BAND FORMATION

In this section, we will present the finite element simulation of plane strain shear band initiation for brittle damage material under compressive loading. Many studies have been done to numerically simulate the shear band phenomenon using large deformation theory. Tvergaard et al. (1981) analyzed a plane strain tension test using a finite element model based on a phenomenological corner theory proposed by Christoffersen and Hutchinson (1979). Heinstein and Yang (1992) presented a finite element simulation of shear band formation during metal forming using a modified Gurson yield function and combined isotropic-kinematic hardening. More recently, Ramakrishnan and Atluri (1994) used a dual yield constitutive model to carry out a set of finite element simulations of the shear band formation in plane strain tension as well as compression.

It is our intention here to illustrate the qualitative behavior of the shear band

formation in the regime of infinitesimal strain for brittle material, therefore, we do not emphasize the theoretical background on the development of the finite element formulation. The computation was carried out using the commercial code ABAQUS. Polycrystalline ice is analyzed and the material constitutive behavior is again governed by Equations (15) and (16). The option UMAT is used in the input data card and a user material interface subroutine is written to describe the material constitutive behaviors.

An 8-node 16-d.o.f. plane strain element with reduced integration is used. The undeformed specimen geometry is shown in Figure 6. The middle node C is constrained in both the x_1 and x_2 directions. The node at B is constrained only in the x_1 direction. The top surface and the bottom surface are subjected to step-wise incremental displacements toward each other to simulate compression loading. To trigger the formation of the shear band, initial imperfection in the form of inhomogeneous stiffness is introduced. The five elements on the diagonal plane passing through C were made weaker by reducing the diagonal terms of the stiffness matrix for Equation (16) by 1%. The deformed configuration of the simulated specimen is shown in Figure 7.

One of the limitations of the finite element simulation, as indicated by many researchers (Heinstein and Yang 1992; Ramakrishnan and Atluri 1994), is that the solution (such as the band width) is strongly dependent on the finite element mesh. As pointed out by Asaro and Needleman (1984), these limitations are not inherent to the continuum description, but are consequences of its application to (piecewise) homogeneous and homogeneously deformed material elements. By

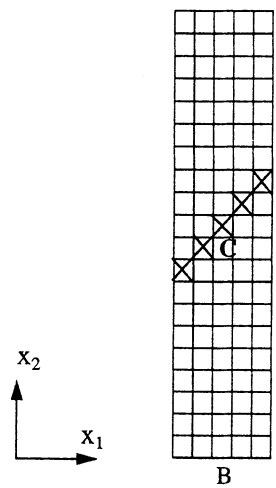

Figure 6. *Plane strain shear band initiation (undeformed configuration).*

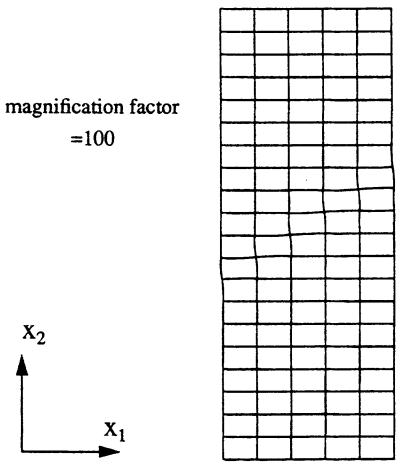

Figure 7. *Plane strain shear band initiation (deformed configuration).*

carryout out a full solution to the relevant boundary value problem, regions of localization propagate from strain concentrations and deformation field gradients introduce an implicit length scale. The mesh dependency is of less importance in the present study, since the brittle nature of the damage materials determines that once the macroscopic shear band occurs, the load bearing capacity of the whole specimen may decrease dramatically.

CONCLUSIONS

A fracture of brittle solids in monotonic compression was reviewed by Argon et al. (1983). The fracturing mechanisms have been studied from both the extrinsic and intrinsic points of view. In an *extrinsic* mode of fracture, large preexisting cracks comparable with the dimensions of the part can extend under uniaxial compression or constrained compression when the displacement of the crack surfaces provides sufficient opening displacements at the crack tips. In contrast, *intrinsic mode* views shear faulting in compression to be the result of an evolutionary localization process involving *en echelon* action of cracks. The mechanistic models were related to the phenomenological developments in dilatational plasticity. The present work, however, identifies itself from the previous plasticity approach in that it accounts for the damage of the material as an evolution of its elastic stiffness properties. Formulations of the nonlinear constitutive relations used here remains within the range of infinitesimal strains. When deformations within the shear band are unstable, such formulations provide an alternative description of the initiation of the intrinsic mode of fracture. The authors believe this provides a better quantitative understanding of the failure modes of

some brittle solids in compression. Furthermore, as pointed out by Ortiz (1987), the localization analyses are highly sensitive to the details of the constitutive equations, therefore, this type of stability analysis will provide a valuable tool in assessing the accuracy of differential material models.

Fundamentally, continuum damage mechanics seeks to provide constitutive descriptions for solids with innumerable cracks, yet bears in mind that the macroscale response is governed by the microstructural evolution. The linkage of the microstructural physics to the damage model is provided through the damage evolution equations. The damage mechanics models offer a macroscale representation of the microstructural response of a material; the shear band formation discussed in this paper is thus a representation of the loss of uniqueness of the macroscale homogeneous deformation. Microstructural analyses of brittle materials containing cracks are known to exhibit microstructural instabilities. This study addresses an alternative instability that can also arise: loss of stablity of deformation process may occur on the macroscale while the microcracks are themselves locally stable. The instabilities are shown to occur at infinitesimal strain levels with little degradation of the elastic axial stiffness prior to localization. The initiation of localized deformation is thus an important consideration in establishing material parameters and constitutive equations used in damage modelling.

ACKNOWLEDGEMENT

Research support provided by the Office of Naval Research through Grant No. DOD-N00014-94-1-1192 to the University of Michigan is gratefully acknowledged.

REFERENCES

Anand, L. 1984. *Scripta METALLURGICA,* 18:423-427.

Argon, A. S., A. A. Bradd, J. D. Embury, A. G. Evans, J. W. Hutchinson, W. H. Lewis, D. L. Sikarskie and T. F. Wong. 1983. *Fracture in Compression of Brittle Solids,* Comm. on Fracture in Compressive Stress Fields, NMAB-404, Washington, D.C.: Nat. Ac. Press.

Asaro, R. J. and A. Needleman. 1984. *Scripta METALLURGICA,* 18:429-435.

Ashby, M. F. and S. D. Hallam. 1986. *Acta Metall.*, 34:497-510.

Becker, R. 1987. *J. Mech. Phys. Solids,* 35(5):577-599.

Becker, R. and A. Needleman. 1986. *J. Appl. Mech.*, 53:491-499.

Brown, L. M. and J. D. Embury. 1973. *Proc. 3rd Int. Conf. on Strength of Metals and Alloys.*, Inst. Metals, London, p. 164.

Chow, C. L. and F. Yang. 1991. *Eng. Fracture Mechanics,* 40(2):335-343.

Christoffersen, J. and J. W. Hutchinson. 1979. *J. Mech. Phys. Solids,* 27:465-487.

Coleman, B. D. and M. E. Gurtin. 1967. *J. Chem. Phys.*, 47:597-613.

Darve, F. 1984. *Mechanics of Engineering Materials,* Chapter 9, pp. 179-197.

Darve, F., E. Flavigny and M. Meghacou. 1995. *Computers and Geotechnics,* 17(2):203-224.

Davidson, L. and A. L. Stevens. 1973. *J. Appl. Phys.*, 44(2):668-674.

Goods, S. H. and L. M. Brown. 1979. *Acta Meta.*, 27:1–15.

Gurson, A. L. 1977. *J. Engineering Materials and Technology*, 99:2–15.

Hawkes, I. and M. Mellor. 1972. *Journal of Glaciology*, 11(61):103–131.

Heinstein, M. W. and H. T. Y. Yang. 1992. *Int. J. Numerical Methods in Eng.*, 33:719–737.

Hild, F., P. Larsson and F. Leckie. 1992. *Int. J. Solids Structures*, 29(24):3221–3238.

Hill, R. 1958. *J. Mech. Phys. Solids*, 6:236–249.

Horii, H. and S. Nemat-Nasser. 1986. *Phil. Trans. R. Soc. Lond.*, A319:337–374.

Kachanov, L. M. 1958. *Izv. Akad. Nauk USSR Otd. Tekh. Nauk*, 8:26–31.

Kachanov, M. 1993. *Advances in Applied Mechanics*, 30:259–445.

Kachanov, M. 1994. *Int. J. Damage Mechanics*, 3(4):329–337.

Karr, D. G. and K. Choi. 1989. *Mechanics of Materials*, 8:55–66.

Karr, D. G. and X. Sun. 1995. *Int. J. Offshore Polar Engineering*, 5:23–31.

Krajcinovic, D. 1982. *Int. J. Solids Structures*, 18(7):551–562.

Krajcinovic, D. 1989. *Mechanics of Materials*, 8:117–197.

Krajcinovic, D., M. Basista and D. Sumarac. 1991. *J. Appl. Mech.*, 58:305–310.

Krajcinovic, D. and G. U. Fonseka. 1981. *J. Appl. Mech.*, 48:809–824.

Krajcinovic, D. and S. Selvaraj. 1983. *Proc. Inc. Conf. on Constitutive Laws for Engineering Materials*, C. S. Desai and R. H. Gallagher, eds., Tucson, pp. 399–406.

Lubarda, V. A. and D. Krajcinovic. 1993. *Int. J. Solids Structures*, 30(20):2859–2877.

Mills, L. L. and R. M. Zimmerman. 1970. *ACI Journal*, October, 802–807.

Needleman, A. 1979. *J. Mech. Phys. Solids*, 27:231–254.

Neilsen, M. K. and H. L. Schreyer. 1992. *Engineering Mechanics*, edited by Loren D. Lutes and John M. Niedzwecki. *Proceedings of the Ninth ASCE Conference*, College Station, Texas.

Neilsen, M. K. and H. L. Schreyer. 1993. *Int. J. Solids Structures*, 30(4):521–544.

Ortiz, M. 1987. *Mechanics of Materials*, 6:159–174.

Pietruszczak, S. and G. Xu. 1995. *Int. J. Solids Structures*, 32(11):1517–1533.

Ramakrishnan, N. and S. N. Atluri. 1994. *Mechanics of Materials*, 17:307–317.

Rice, J. R. 1976. in *Theoretical and Applied Mechanics*, Proceedings of the 14th IUTAM Congress, Delft, 30 August to 4 September, pp. 207–220. W. T. Koiter, ed., North-Holland Publishing Company.

Rizzi, E., I. Carol and K. Willam. 1995. *Journal of Engineering Mechanics*, 121(4):541–554.

Rudnicki, J. W. and J. R. Rice. 1975. *J. Mech. Phys. Solids*, 23:371–394.

Schulson, E. M. 1990. *Acta Metall. Mater.*, 38(10):1963–1976.

Schulson, E. M., M. C. Gies, G. J. Lasonde and W. A. Nixon. 1989. *J. Glaciol.*, 35(121):378–382.

Shah, S. P. 1984. *Mechanics of Engineering Materials*, Chapter 29, pp. 579–590.

Stören, S. and J. R. Rice. 1975. *J. Mech. Phys. Solids*, 23:421–441.

Sun, X. 1995. *Constitutive Bifurcation and Shear Band Initiation of Rate Independent Brittle Damage Materials*, Ph.D. thesis, the University of Michigan, Department of Naval Architecture and Marine Engineering, Ann Arbor, Michigan.

Tugcu, P. 1993. *Int. J. Non-Linear Mechanics*, 28(4):385–392.

Tvergaard, V. 1981. *Int. J. Fract.*, 17(4):389–407.

Tvergaard, V. 1987. *M. Mech. Phys. Solids*, 35(1):43–60.

Tvergaard, V. and A. Needleman. 1984. *Acta Meta.*, 32:157–169.

Tvergaard, V., A. Needleman and K. K. Lo. 1981. *J. Mech. Phys. Solids*, 29(2):115–142.

Yamamoto, H. 1978. *Int. J. Fract.*, 14:347–365.